Proceedings 10th NUMGE 2023
10th European Conference on Numerical Methods in Geotechnical Engineering
Zdravkovic L, Kontoe S, Taborda DMG, Tsiampousi A (eds)

https://doi.org/10.53243/NUMGE2023-54

Numerical modelling of a shallow tunnel buried adjacent to a surface structure in liquefiable ground

J. Zhang[1], E. Bilotta[2]

[1]*Department of Civil Engineering, Xi'an Jiaotong University, Xi'an, China*
[2]*Department of Civil, Architectural and Environmental Engineering, University of Naples Federico II, Naples, Italy*

ABSTRACT: Earthquake-induced liquefaction is likely to cause uplift displacements of underground structures and excessive settlements of surface structures. While these two phenomena have been investigated separately in the literature, the case of a shallow tunnel buried adjacent to a surface structure in liquefiable ground remains to be thoroughly studied. In this paper, the OpenSees platform is employed to numerically model a centrifuge test on a tunnel-structure system in saturated Hostun sand. The PM4Sand constitutive model is calibrated to capture the nonlinear behaviours of the liquefiable ground. Overall, the numerical analysis is in good agreement with the centrifuge test data. The excess pore pressure build-up, the acceleration responses of the Hostun sand, the vertical uplift of the tunnel, and the settlements of the surface structure all are simulated with adequate accuracy. The validated numerical model is then used to investigate the boundary effect of the rigid container adopted in the centrifuge tests.

Keywords: liquefaction; tunnel; surface structure; OpenSees; boundary effect

1 INTRODUCTION

Earthquake-induced liquefaction is a major concern for the seismic safety of all engineering structures. Although numerous studies have been dedicated to the topic, the underground and the surface structures are usually investigated separately (Adamidis and Madabhushi, 2018; Shen et al., 2022). The interaction between underground and surface structures in liquefiable soil has only recently become the focus of intensive academic research (Zhu et al., 2021a, 2021b).

The purpose of this paper is to continue the research on the subject matter employing the OpenSees platform (Pacific Earthquake Engineering Research Centre, 2021). A two-dimensional numerical model is constructed consisting of a rectangular tunnel and an adjacent surface structure in liquefiable Hostun sand. The numerical model is validated against the centrifuge test data gathered by Miranda (2019). Then, it is used to investigate the boundary effect of the rigid container adopted in the centrifuge tests.

2 THE CENTRIFUGE TESTS

A series of centrifuge shaking tests were carried out using the Turner Beam Centrifuge at the Schofield Centre in the University of Cambridge. Four models were tested, of which only the second one, namely Model 2, is relevant in this paper.

The test was conducted under a centrifugal acceleration of 60*g*. Thus, the physical model imitated a prototype 60 times larger, and all the specifications elaborated herein will be in the prototype scale unless stated otherwise. As illustrated in Figure 1, a rectangular tunnel was buried in saturated Hostun sand. The cross-section of the tunnel was 4.6 m in height and 9.2 m in width, and it was made of aluminium of a uniform thickness that was 180 mm. The total mass of the tunnel was 4.1×10^5 kg. A surface structure, also made of aluminium, was situated adjacent to the tunnel. It was single-storey and weighed 2.1×10^5 kg.

A rigid container was adopted, and two absorbent layers of Duxseal material were attached to the lateral sides to reduce the boundary effect (Adamidis and Madabhushi, 2018; Chian et al., 2014). An aqueous solution of hydroxypropyl methylcellulose, with a viscosity 60 times that of water, was used to saturate the Hostun sand, therefore ensuring compatibility between the diffusion and the dynamic time.

3 THE NUMERICAL MODEL

3.1 Calibration of the constitutive model

The plasticity model PM4Sand (Version 3.1) is employed to simulate the responses of the liquefiable Hostun sand (Boulanger and Ziotopoulou, 2017).

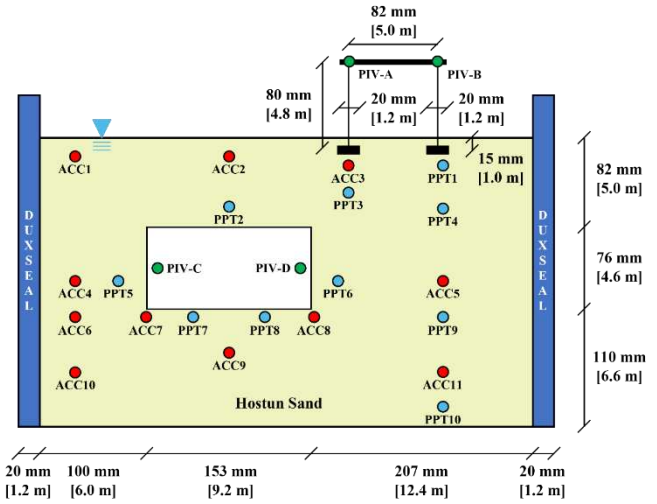

Figure 1. Layout of Model 2 of the centrifuge tests with prototype scale dimensions in brackets (modified after Miranda et al. 2021)

In OpenSees, 24 constitutive parameters are required to create a PM4Sand material. The default correlations set by the developers have been invoked for 14 of them. The other 10 parameters plus the permeability coefficient are the main targets of the calibration process, as listed in Table 1.

Table 1. Constitutive parameters for PM4Sand

Parameter	Int. Est.	TRX Cal.	Model 2
D_r	Equation (1)	46%	66%
G_o	Equation (4)	696	774
h_{po}	0.04	0.07	0.07
ρ (Mg / m^3)	Equation (8)	1.94	1.98
e_{max}	1.049	1.049	1.049
e_{min}	0.648	0.648	0.648
ϕ'_{cv}	33.8°	33.8°	33.8°
Q	8.4	8.4	8.4
R	0.78	0.78	0.78
ν	0.31	0.31	0.31
k (m / s)	Equation (9)	1×10^{-3}	8×10^{-5}

The maximum and minimum void ratios of Hostun sand are reported to be e_{max} = 1.049 and e_{min} = 0.648, respectively (Kassas et al., 2021). Thus, the relative density is simply:

$$D_r = (e_{max} - e)/(e_{max} - e_{min}), \quad (1)$$

where e is the current void ratio.

The small-strain shear modulus G_{max} in PM4Sand is dependent on the mean effective stress p according to:

$$G_{max} = G_o p_A (p/p_A)^{0.5}, \quad (2)$$

where p_A is the atmospheric pressure, and G_o is the shear modulus constant. Similarly, an expression for Hostun sand has been proposed by Azeiteiro et al. (2017):

$$G_{max} = 293 \times \frac{(2.97-e)^2}{1+e} p_A \left(\frac{p}{p_A}\right)^{0.49}. \quad (3)$$

By comparing these two equations, G_o could be estimated for Hostun sand by:

$$G_o = 293 \times \frac{(2.97-e)^2}{1+e}. \quad (4)$$

Regarding the critical state line in PM4Sand, it has been defined as (Bolton, 1986):

$$D_{r,cs} = \frac{R}{Q - \ln(100\frac{p}{p_A})}, \quad (5)$$

where $D_{r,cs}$ is the relative density at critical state. Q and R are Bolton's constants, and they are 8.4 and 0.78 for Hostun sand, respectively (Kassas et al., 2021).

The effective friction angle at critical state ϕ'_{cv} is measured to be 33.8° (Kassas et al., 2021). Hence, the Poisson's ratio is obtained via the intermediate of the lateral pressure coefficient K_o by:

$$K_o = 1 - \sin\phi'_{cv} = 0.44, \text{ and} \quad (6)$$

$$\upsilon = \frac{K_o}{1+K_o} = 0.31. \quad (7)$$

The contraction rate parameter h_{po} is set to be 0.04 in Kassas et al. (2021). Although this value is highly case-specific, it provides an initial estimate, from which the calibration process could be started.

The mass density of saturated Hostun sand is:

$$\rho = \frac{\rho_w(G_s+e)}{1+e}, \quad (8)$$

where ρ_w is the mass density of the pore fluid; G_s is the specific gravity of the solids. The former is 1 Mg / m^3, and the latter is measured to be 2.75 in lab test.

The permeability coefficient k is not part of the constitution of PM4Sand, but it is mandatory for the formulation of displacement-pressure (u-p) coupled elements in OpenSees. It could be estimated for Hostun sand based on the equation by Adamidis et al. (2020):

$$k = 2.92 \times 10^{-3} \times \frac{e^3}{1+e} \text{ (m/s)}. \quad (9)$$

To verify the validity of the estimated parameters, undrained cyclic triaxial (TRX) tests were conducted on the Hostun sand. The target initial void ratio was 0.865, corresponding to a relative density of 46%. The samples underwent isotropic consolidation under a cell pressure of 50 kPa. The amplitude of the cyclic deviator stress q ranged between 14.0 kPa and 20.3 kPa, corresponding to cyclic stress ratios (CSR) from 0.137 to 0.200. The samples were considered liquefied once the excess pore pressure (EPP) ratio exceeded 0.9. Thus, a cyclic resistance ratio (CRR) curve was established for the Hostun sand by the CSR and the number of cycles to reach liquefaction N_{liq}.

Because PM4Sand is only available in plane-strain formulation, undrained cyclic direct simple shear (DSS) tests are simulated using the PM4Sand material under the initial effective vertical stress of 50 kPa. With a void ratio of 0.865, the relative density D_r, the shear modulus constant G_o, the mass density ρ, and the permeability coefficient k of the Hostun sand could all be estimated by the pertinent equations. The contraction rate parameter h_{po} is then calibrated to match the CRR vs. N_{liq} curve obtained from the TRX lab tests. It must be pointed out that the CRR data are not directly comparable between the DSS and the TRX tests. The following conversion is necessary (Castro, 1975):

$$\mathrm{CRR_{DSS}} = \frac{2(1+2K_o)}{3\sqrt{3}}\mathrm{CRR_{TRX}}. \qquad (10)$$

The comparison between the $\mathrm{CRR_{DSS}}$ converted from the TRX lab tests and the $\mathrm{CRR_{DSS}}$ simulated using PM4Sand is shown in Figure 2. The dashed lines are the fitting curves of the data points of the same color. When N_{liq} is between 10 and 30, the numerical DSS tests have yielded satisfactory results. That range corresponds to an earthquake magnitude of 7 to 8 (Seed and Idriss, 1971), which is the target seismicity level of the centrifuge tests.

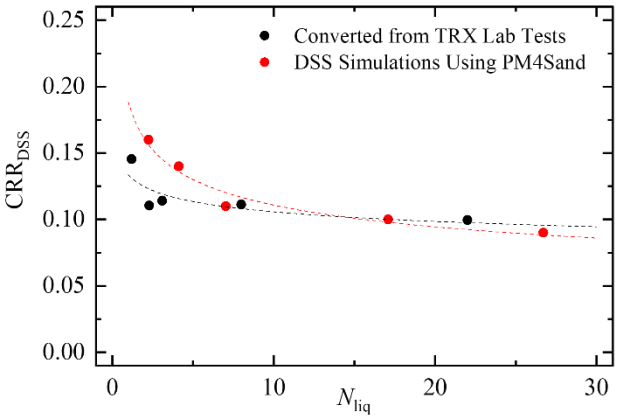

Figure 2. The converted and the simulated $\mathrm{CRR_{DSS}}$ *vs.* N_{liq} *curves*

3.2 *Modelling of the centrifuge test*

The accelerogram recorded at the base of the rigid container and its Fourier spectrum are shown in Figure 3 in prototype scale. The energy of the signal is mainly carried by the 10 near-sinusoidal cycles of 1 Hz, and the peak acceleration is 0.43g.

The initial void ratio of the Hostun sand was 0.792. However, this was measured immediately after Model 2 was prepared in 1g environment. Preliminary numerical analyses indicate that the void ratios at the beginning of the shaking is larger than that at the very beginning of the centrifuge tests. The resulting increase in D_r is about 2%. Therefore, the initial relative density of the Hostun sand is set to be 66%.

When the centrifuge basket was swung up, an air hammer test was performed, so a profile of the shear wave velocity of the Hostun sand could be obtained. This profile is used to adjust the small-strain shear modulus predicted by Equation (2), so the G_o adopted in the numerical simulation is 744, slightly smaller than what Equation (4) dictates.

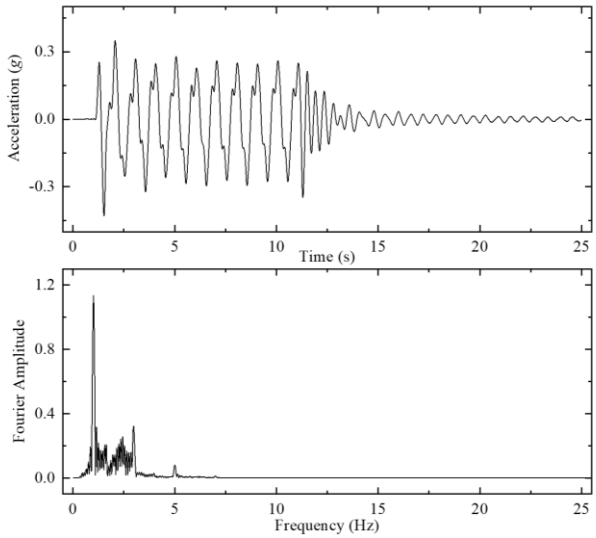

Figure 3. Input excitation for Model 2 in prototype scale

According to Equation 9, the permeability coefficient of the Hostun sand should be 7.9×10^{-4} m / s. Although the yielded numerical results are acceptable, it is outperformed by the back-calculated permeability coefficient of 8×10^{-5} m / s in simulating the dissipation of the EPP and the uplift of the tunnel, especially after 12.5 s. Hence, the latter is adopted in the following analyses.

The finite element mesh of Model 2 is illustrated in Figure 4. The hosting medium is modelled by quadrilateral *u-p* coupled elements termed as SSPquadUP elements (McGann et al., 2012). While the Hostun sand has been assigned the PM4Sand material, the Duxseal laterals are assumed to be elastic and isotropic, with a Young's modulus of 800 kPa, a mass density of 1.65 Mg / m^3, and a Poisson's ratio of 0.46. A nominal element size of 0.5 m is chosen, rendering the Hostun sand and the Duxseal laterals in 1722 elements.

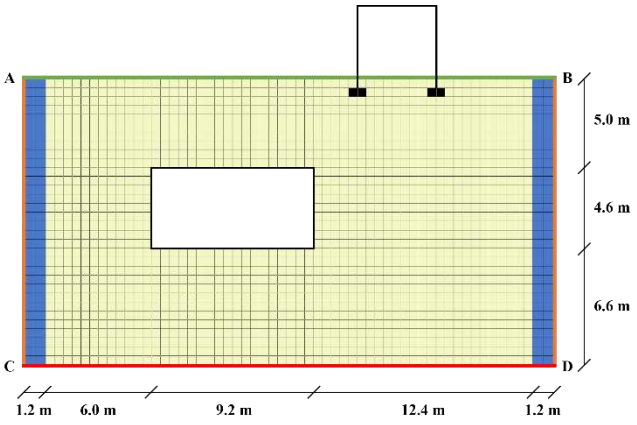

Figure 4. Finite element mesh of Model 2

Inside the Hostun sand, there are 4 elements constituting the foundations of the surface structure, and they are assigned the stiffness and mass properties of the aluminium material. The columns and the roof of the surface structure are modelled by beam elements. Around the perimeter of the rectangular hollow is defined the lining of the tunnel. It consists of 54 beam elements, whose nodal displacements are equalled to those of the adjoining elements of the Hostun sand. The material properties are a Young's modulus of 7×10^4 MPa and a linear mass density of 15 Mg / m.

The entire model is supported by the vertical constraints on the bottom edge CD, and free drainage is defined on the upper edge AB. The application of the rigid container in the centrifuge tests meant that the input excitation came from the side walls as well as the base. That is achieved in OpenSees by a UniformExcitation load pattern and horizontal fixes on the nodes of the three encasing boundaries, namely AC, BD, and CD.

The viscoelastic dissipative property of the soil-structure system is represented by mass and stiffness proportional Rayleigh damping with 0.5% damping ratio at the frequencies of 1 Hz and 3 Hz.

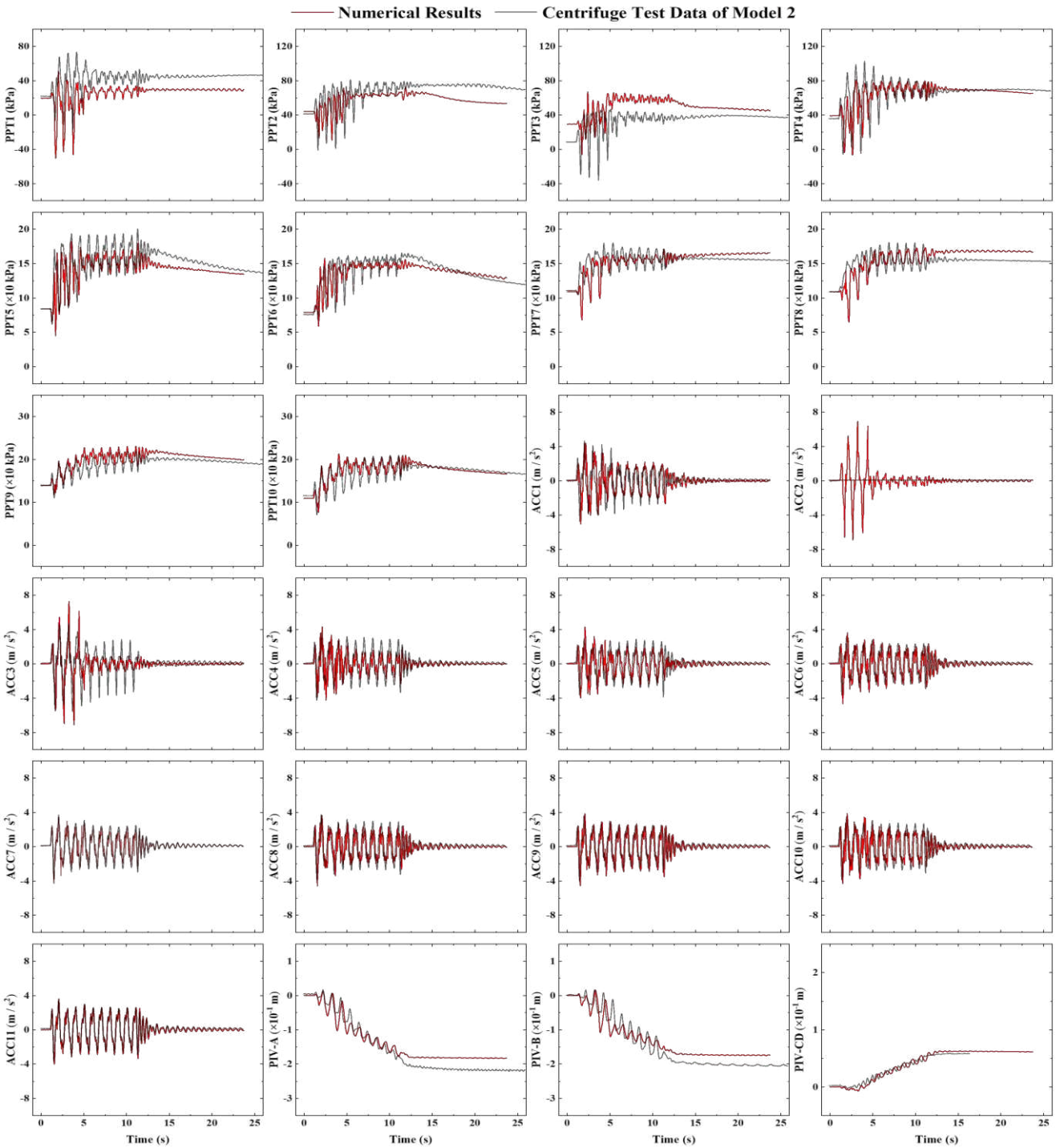

Figure 5. Comparison between the numerical results (red line) and the centrifuge test data (black line)

3.3 *Comparison between the numerical results and the centrifuge test data*

The numerical simulation is performed in two stages. The first stage concerns the computation of the geostatic stresses. The second stage is the seismic analysis, where the model is subject to horizontal shaking.

Dynamic responses of the model during the second stage are generated at the positions of the sensors as marked in Figure 1. They include the pore pressure data of PPT#, the acceleration responses of the Hostun sand of ACC#, the settlements of PIV-A and PIV-B, and the uplifts of the tunnel, which is the average vertical displacements of PIV-C and PIV-D, denoted as PIV-CD. A comparison between the numerical results and the centrifuge test data is presented in Figure 5.

The acceleration comparisons exhibit generally good agreement, except that ACC2 malfunctioned during the test and did not return any meaningful data. The vertical propagation of the shear wave is greatly impeded when the Hostun sand liquefies after four to five seconds of shaking. The abrupt transition from amplification to attenuation is especially pronounced at ACC2 and ACC3. Although ACC1 is buried at the same depth, it is much closer to the side wall of the rigid container, which also functions as a source of input excitation. Therefore, ACC1 is less affected by the liquefaction of the sand.

While the uplifts of the tunnel are very well matched, the numerically computed settlements of the surface structure are smaller than what is detected in the centrifuge test. The error is about 15%. In model scale, the absolute error is less than 0.75 mm.

The pore pressure data from the centrifuge tests are reproduced by the numerical models with reasonable accuracy. However, the numerical data at PPT3 are obviously too large. This has been attributed to the dislocation of the pore pressure transducer. When Model 2 was dissected after the centrifuge tests, PPT3 was found at a depth much shallower than its intended position.

Thus, the numerical model is validated against the centrifuge test data, and it is used to facilitate further discussions on the boundary effect of the rigid container.

4 BOUNDARY EFFECT OF THE RIGID CONTAINER

The rigid container was adopted in the centrifuge tests to permit high speed photogrammetry, so the movements of four crucial positions could be tracked by particle image velocimetry (PIV). Although two Duxseal laterals were attached to the side walls, the boundary effect of the rigid container is still present, as has been seen on the acceleration responses of ACC1.

To clarify the boundary effect of the rigid container, a widened numerical model is built and computed. Compared with the one in Figure 4, it is different in three ways. Firstly, it has a width of 100 m, which is thrice that of Model 2. Secondly, the Duxseal laterals are cancelled, and the entire hosting medium is made of Hostun sand. Thirdly, periodical boundary conditions are defined on the two lateral edges, namely AC and BD.

According to the numerical results, the EPP accumulation in the rigid container is much slower than that in the widened model with periodical boundaries. Typically, the Hostun sand in the former case would reach the same degree of liquefaction 2 to 3 s later. In addition, the distribution pattern of the EPP is also different as demonstrated by the comparison of Figure 6 and Figure 7. The contour in the latter is almost symmetric about the vertical centre line of the tunnel, expect for some minor deviations at the positions of the foundations of the surface structure. This is a more realistic simulation of a ground subject to vertically propagating shear waves. In contrast, a very clear influence of the two lateral boundaries could be seen in Figure 6. The EPP on the left side is significantly larger than that on the right side. This means that while the Hostun sand is being compressed by the left wall, it is dilating at the opposite side. Consequently, the overall accumulation of EPP is also milder in Figure 6. During the entire simulated period, the maximum EPP in the rigid container and the widened model with periodical boundaries are 307 kPa and 330 kPa, respectively.

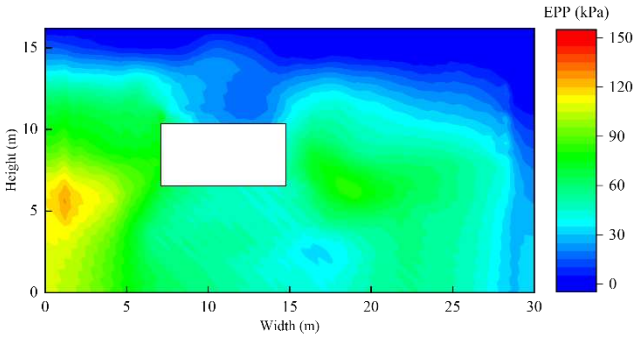

Figure 6. EPP contour in rigid container at 12 s

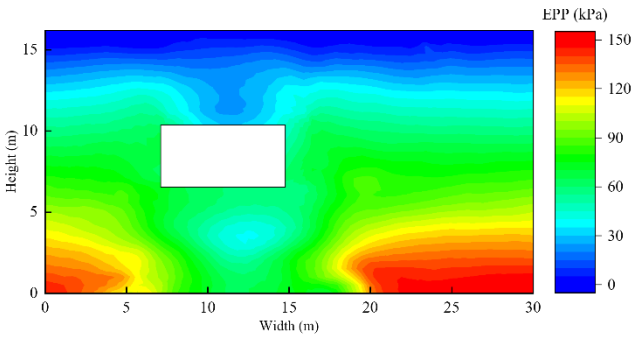

Figure 7. EPP contour in the widened model at 12 s

A third numerical model is computed, which has the same dimensions as shown in Figure 4. Like in the widened model, the Duxseal material is replaced by Hostun sand, and periodical boundary conditions are defined on the two lateral sides. This third model could be considered a numerical variation of Model 2 in a laminar box.

As shown in Figure 8, a direct result of the relatively mitigated liquefaction in the rigid container is that the uplift displacements of the tunnel are greatly reduced. Not only the uplift is much slower in the rigid container, the maximum value only reaches a quarter of those in the other two cases.

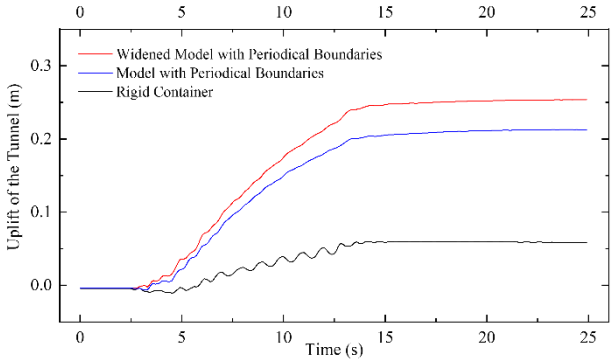

Figure 8. Tunnel uplift with different boundary conditions

5 CONCLUSIONS

A two-dimensional plane-strain numerical model is constructed employing the OpenSees platform. The model consists of a rectangular tunnel and an adjacent surface structure in saturated Hostun sand.

The constitutive model PM4Sand is calibrated to capture the nonlinear behaviour of the liquefiable ground. It has been demonstrated that the numerical simulation could reproduce the data of a centrifuge shaking test with reasonable accuracy.

The numerical soil-structure system is then used to investigate the boundary effect of the rigid container adopted in the centrifuge test. It proves that the liquefaction of the Hostun sand is relatively mitigated by the rigid container. However, this does not affect the significance of the centrifuge data as a benchmark to verify the validity of numerical models.

6 ACKNOWLEDGEMENTS

The research was supported by the National Natural Science Foundation of China (52108383), the China Postdoctoral Science Foundation (2021M702626), the State Key Laboratory of Disaster Reduction in Civil Engineering (SLDRCE21-02), and the Fundamental Research Funds for the Central Universities (xzy012022075). The authors also acknowledge the computational resources provided by the HPC platform of Xi'an Jiaotong University. The benchmark centrifuge test is part of the project STILUS funded by the network SERA (Seismology and Earthquake Engineering Research Infrastructure Alliance for Europe, EC grant agreement No. 730900). The authors acknowledge the staff of the testing facility, the Schofield Centre at Cambridge (UK), and its Director Professor Gopal Madabhushi.

7 REFERENCES

Adamidis, O., Alber, S., Anastasopoulos, I. 2020. Assessment of the three-dimensional printing of granular media for geotechnical applications, *Geotechnical Testing Journal* **43**, 641-659.

Adamidis, O., Madabhushi, S. P. G. 2018. Deformation mechanisms under shallow foundations on liquefiable layers of varying thickness, *Géotechnique* **68**, 602-613.

Azeiteiro, R. J. N., Coelho, P. A. L. F., Taborda, D. M. G., Grazina, J. C. D. 2017. Critical state-based interpretation of the monotonic behavior of Hostun sand, *Journal of Geotechnical and Geoenvironmental Engineering* **143**, 04017004.

Bolton, M. D. 1986. The strength and dilatancy of sands, *Géotechnique* **36**, 65-78.

Boulanger, R. W., Ziotopoulou, K. 2017. *PM4Sand (Version 3.1): A sand plasticity model for earthquake engineering applications*, University of California, California.

Castro, G. 1975. Liquefaction and cyclic mobility of saturated sands, *Journal of the Geotechnical Engineering Division* **101**, 551-569.

Chian, S. C., Tokimatsu, K., Madabhushi, S. P. G. 2014. Soil liquefaction-induced uplift of underground structures: physical and numerical modeling, *Journal of Geotechnical and Geoenvironmental Engineering* **140**, 04014057.

Kassas, K., Adamidis, O., Gerolymos, N., Anastasopoulos, I. 2021. Numerical modelling of a structure with shallow strip foundation during earthquake-induced liquefaction, *Géotechnique* **71**, 1099-1113.

McGann, C. R., Arduino, P., Mackenzie-Helnwein, P. 2012. Stabilized single-point 4-node quadrilateral element for dynamic analysis of fluid saturated porous media, *Acta Geotechnica* **7**, 297-311.

Miranda, G. 2019. *Soil-tunnel-building interaction in a soil susceptible to liquefaction*, University of Naples Federico II, Italy. (in Italian)

Miranda, G., Nappa, V., Bilotta, E., Haigh, S. K., Madabhushi, S. P. G. 2021. Centrifuge tests on tunnel-building interaction in liquefiable soil. *Proceedings of the Tenth International Symposium on Geotechnical Aspects of Underground Construction in Soft Ground* (Eds: Elshafie, M., Viggiani, G. & Mair, R.), 613-619. CRC Press, London.

Pacific Earthquake Engineering Research Center. 2021. *User Documentation.* https://opensees.berkeley.edu/

Seed, H. B., Idriss, I. M. 1971. Simplified procedure for evaluating soil liquefaction potential, *Journal of the Soil Mechanics and Foundations Division* **97**, 1249-1273.

Shen, Y., Zhong, Z., Li, L., Du, X., Naggar, M. H. 2022. Seismic response of shield tunnel structure embedded in soil deposit with liquefiable interlayer, *Computers and Geotechnics* **152**, 105015.

Zhu, T., Hu, J., Zhang, Z., Zhang, J., Wang, R. 2021a. Centrifuge shaking table tests on precast underground structure-superstructure system in liquefiable ground, *Journal of Geotechnical and Geoenvironmental Engineering* **147**, 04021055.

Zhu, T., Wang, R., Zhang, J. 2021b. Effect of nearby ground structures on the seismic response of underground structures in saturated sand, *Soil Dynamics and Earthquake Engineering* **146**, 106756.